Tuning Electronic and Proton Transfer Properties on Amino-Functionalized Co-based MOF for Efficient Photocatalytic Hydrogen Evolution

Yollada Inchongkol,[†] Taya Ko Saothayanun,[†] Kanyaporn Adpakpang,[†] Natchaya Phongsuk,[†] Sarawoot Impeng,[‡] Soracha Kosasang,[⊥] Nattapol Ma,[§] Satoshi Horike,[⊥] and Sareeya Bureekaew[†]*

[†] School of Energy Science and Engineering, Vidyasirimedhi Institute of Science and Technology, Rayong 21210, Thailand

[‡] National Nanotechnology Center (NANOTEC), National Science and Technology Development Agency (NSTDA), 111 Thailand Science Park, Pahonyothin Rd., Klong Luang, Pathum Thani 12120, Thailand

[⊥] Department of Chemistry, Graduate School of Science, Kyoto University, Kitashirakawa-Oiwakecho, Sakyo-ku, Kyoto 606-8502, Japan

[§] International Center for Young Scientists (ICYS), National Institute for Materials Science, 1-1 Namiki, Tsukuba, Ibaraki, 305-0044, Japan

[⊥] Department of Materials Science and Engineering, School of Molecular Science and Engineering, Vidyasirimedhi Institute of Science and Technology, Rayong 21210, Thailand

*E-mail: sareeya.b@vistec.ac.th

KEYWORDS: Metal-Organic Framework, Water Splitting, Photocatalysis, Hydrogen Production, Cocatalyst, Proton Diffusion

ABSTRACT Efficient hydrogen (H_2) production through photocatalytic water splitting was achieved using an amino-functionalized azolate/cobalt-based metal-organic framework (MOF). While previous reports highlighted the amino group's role only as a substituent group for enabling light absorption of MOFs in the visible region, our present study revealed its dual role. The amino substituent not only acts as an electron donor to increase the electron availability at the active Co sites, but also provides hydrogen-hopping sites within the pore channel, facilitating proton (H^+) diffusion along the framework. This dual functionality significantly boosts the performance of this Co-MOF as a hydrogen evolution cocatalyst. When combined with fluorescein and triethylamine as the photosensitizer and sacrificial agent, respectively, the Co-MOF achieved a remarkable H_2 production rate of 27 mmol g^{-1} over 4 hours. Notably, this performance surpasses that of benchmark platinum (Pt) and titanium dioxide (TiO_2) cocatalysts.

INTRODUCTION

Hydrogen (H_2) has been considered a clean energy source with environmental benefits and has been suggested to replace fossil fuels. This is due to its high energy density (142 MJ kg^{-1}) and environmentally friendly CO_2-free combustion process. However, the current technology for the production of H_2 still relies on petroleum-based fuels, inevitably releasing greenhouse gases.[1, 2] Photocatalytic water splitting offers alternatives for producing sustainable and greener H_2 to reach net zero emissions by using photocatalysts and renewable resources such as solar light and water.[3,

[4] Generally, semiconductors such as titanium dioxide (TiO_2) are used as photocatalysts to produce H_2 through water-splitting reactions. However, the photocatalytic efficiency of TiO_2 still remained relatively low due to many factors including fast electron-hole recombination rates, poor and unselective catalytic sites, and a wide bandgap that only allows absorption in UV light.[5-7] Several strategies have been developed to promote the H_2 evolution reaction (HER) on the TiO_2 surface. Among them, surface modification by cocatalyst is among the frequently used strategies. Cocatalysts can help boost charge separation, provide more active sites, and lower the activation energy (overpotential) for HER.[8] Typically, noble metal nanoparticles (*e.g.*, Pt and Rh) have been employed as benchmark HER cocatalysts because of their suitable catalytic and electronic properties.[9-14] However, these properties were greatly determined by structural factors such as size, shape, homogeneity, *etc*. Precise control over these factors remains challenging.

Metal-organic frameworks (MOFs), a class of porous coordination polymers constructed from metal nodes and organic linkers, have drawn significant attention in this field due to their high porosity and flexibility in tuning functions through metal/ligand modulation. Because of the potential to incorporate organic linkers that can be functionalized for visible light absorption, MOFs are regularly utilized as photosensitizers to efficiently harness light energy, generating photoexcited electrons for HER. These photoexcited electrons can either participate in the reaction within the framework[15-17] or be transferred to cocatalysts for catalyzing the reaction.[18, 19] Although some MOFs are unable to create long-lived photoexcited electrons, they can function effectively as cocatalysts.[20] This role enables the HER at redox-active catalytic sites, typically transition metal ions, by receiving photoexcited electrons from a light absorber (or photosensitizer). The abundance of single-site catalytic attributes in MOFs is beneficial for photocatalytic H_2 production, providing potential to genuinely get rid of problems faced by particulate cocatalysts such as nanoparticle

aggregation. Moreover, the porosity of MOFs enhances the efficiency of reactant and product diffusion. As a result, MOF-based photocatalytic systems offer advantages in both the rate and quantity of H_2 production.

Several approaches have been explored to enhance the photocatalytic production of H_2 in MOF systems, and one of these approaches involves ligand functionalization. The focus lies on introducing amino substituents onto carboxylate linkers to enhance the light absorption capability of photoactive NH_2-MIL-25(Ti)[21, 22] and NH_2-UiO-66(Zr)[16, 23], effectively covering the naturally rich visible region. However, when designing MOF as HER cocatalyst, it is crucial to select ligands not only for their ability to improve electronic properties, but also to accelerate the diffusion of reactant, particularly proton (H^+), an important feature that has not been addressed in the context of MOF cocatalysts. In traditional HER studies utilizing highly porous or dense materials, the role of H^+ conduction in improving catalytic efficiency has been overlooked despite their potential significance.

Our previous study discovered that a Co(II)-based azole MOF, Co-trz (trz = 1,2,4-triazole), proved to be an effective cocatalyst for photocatalytic HER due to its robustness and richness of catalytic sites, generating H_2 up to 9.32 mmol g^{-1} in 4 hours in the presence of fluorescein under solar light.[24] Herein, amino functional group is introduced to Co-trz framework, denoted as Co-trz-NH_2 (trz-NH_2 = 3-amino-1,2,4-triazole),[25] providing an effective platform for H^+ diffusion due to its induced acid-base interaction. Incorporating amino groups enhances the polarity of the nanopore channels without affecting the pore window (Figure S1). The lone pair of electrons on the basic -NH_2 group facilitates the efficient diffusion of acidic protons, a reactant for H_2 production, reaching the active site within the framework. Additionally, this modification is somewhat expected to alter the electronic properties of the cocatalyst, affecting the HER

performance. To the best of our knowledge, this is the first example that highlights the impact of H^+ diffusion on HER performance in nanoporous MOFs.

RESULTS AND DISCUSSION

Co-trz-NH_2, obtained from microwave-assisted synthesis, shares a similar structure with Co-trz that possessed two different metal centers: octahedral (Co_{Oh}) and tetrahedral (Co_{Td}) sites (Figure 1a). These sites are responsible for maintaining framework rigidity by forming a one-dimensional (1D) chain structure and serving as photocatalytic active sites, respectively. Powder X-ray diffraction (PXRD) pattern of Co-trz-NH_2 is nearly identical to that of Co-trz, except for the reflection at $2\theta = 12.8°$ that disappeared for Co-trz-NH_2 due to an orientational disorder of Co_{Td} caused by the amino-functionalized triazole (Figure 1b).[25] Rod-shaped particles of Co-trz-NH_2 are presented in scanning electron microscopy (SEM) images (Figure 1c), showing the same morphology (shape and size) as Co-trz achieved by optimized synthetic conditions (see supporting information).

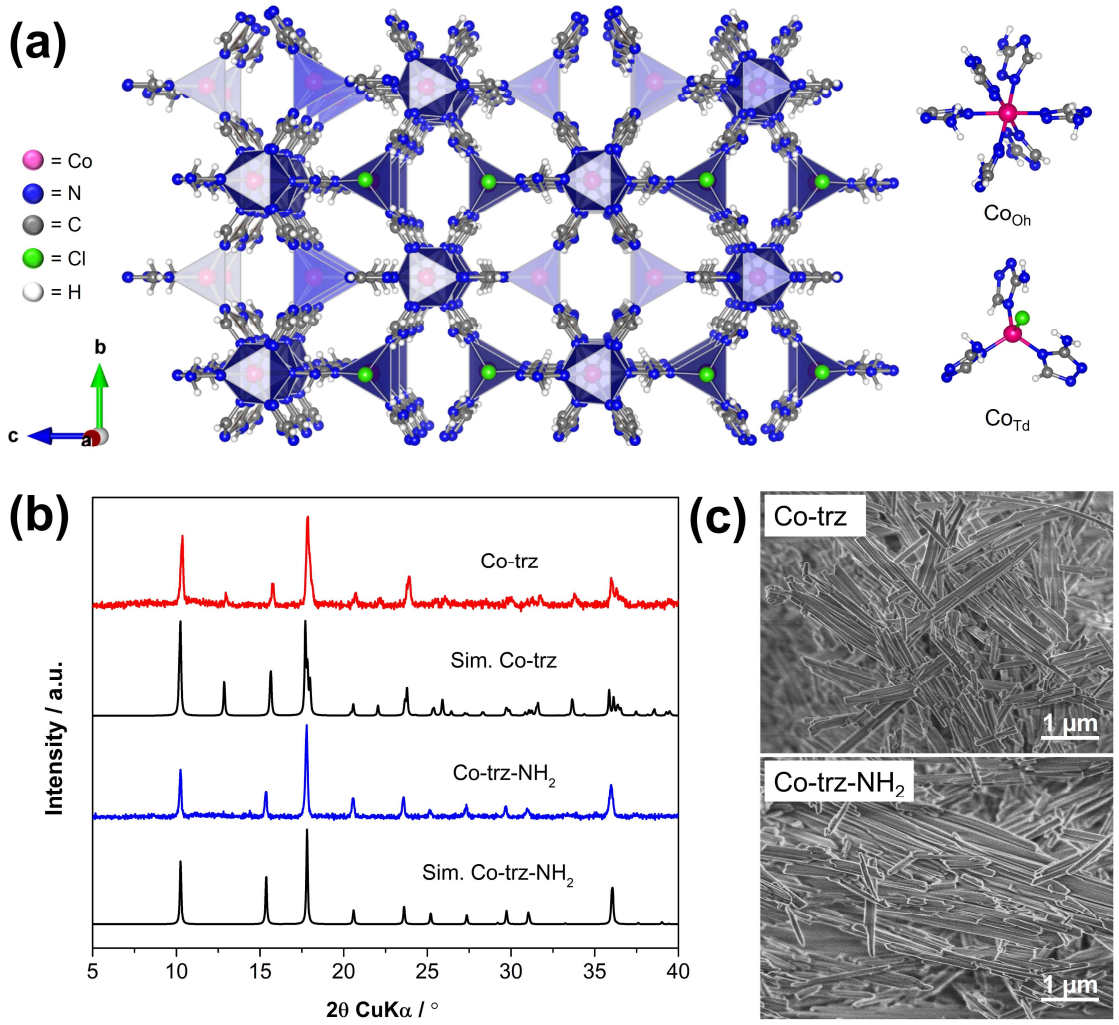

Figure 1. (a) Crystallographic structure of Co-trz-NH_2 consisted two types of coordination geometry for Co^{2+} centers, namely octahedral (Co_{Oh}) and tetrahedral (Co_{Td}), (b) PXRD patterns of as-synthesized Co-trz and Co-trz-NH_2 in comparison to their simulated patterns[25, 26] and (c) SEM images of Co-trz and Co-trz-NH_2.

Photocatalytic experiments were conducted using a solar simulator (100 W Xe lamp equipped with an AM 1.5G filter) as the light source. Similar to the catalytic system of Co-trz, fluorescein (FI) and triethylamine (TEA) were used as a photosensitizer and sacrificial agent, respectively.[24] The catalytic performance of Co-trz-NH_2 was evaluated and compared with that of

Co-trz and the commercial cocatalysts, specifically 10%(w/w) Pt loaded on activated carbon (Pt@C) and TiO_2. The results summarized in Table 1 revealed that the -NH_2 substituent group substantially improves the photocatalytic H_2 production, achieving 27.14 mmol g^{-1} over 4 hours with a rate of 9.05 mmol g^{-1} h^{-1} in Co-trz-NH_2 (by excluding the induction time of approximately an hour). In comparison, the parent Co-trz exhibited 9.23 mmol g^{-1} at 4 hours, with a rate of 3.08 mmol g^{-1} h^{-1} (Figure S2). The H_2 production rate is approximately three times higher when the -NH_2 functionalized ligand is presented, affirming the positive impact of the -NH_2 substituent. In addition, H_2 production did not proceed without a cocatalyst or photosensitizer (Entries 3 and 4), confirming that FI played a role as a photosensitizer and the MOF served as a cocatalyst. Note that the photoexcited electrons from FI can travel through the entire material along the 1D Co_{Oh} chain, enabling the reduction to occur at the Co_{Td} active sites.[24]

The spent Co-trz-NH_2 was further examined using Fourier transform infrared (FT-IR) spectroscopy, PXRD, and SEM, and the results are presented in Figures S3-S5. Prior to the FT-IR measurement, the powders were collected and meticulously washed until the solution reached a neutral pH, ensuring the thorough removal of FI and TEA. The spectra of Co-trz and Co-trz-NH_2 were compared with those of their respective free ligands (trz-H and trz-H-NH_2) as depicted in Figure S3. The free ligands, trz-H and trz-H-NH_2, exhibited strong characteristic peaks at 1480 cm^{-1} and 1590 cm^{-1}, respectively, corresponding to C=N vibrational mode.[27, 28] Upon the formation of the frameworks of Co-trz and Co-trz-NH_2, these characteristic peaks shifted to 1504 cm^{-1} and 1610 cm^{-1}, indicating the coordination of the azolate ligands with Co^{2+} ions. The FT-IR spectra of the utilized materials from the 4-hour reaction remained similar to their fresh counterparts, suggesting the maintenance of coordination between ligands and Co^{2+} ions within the structures. This result suggests the stability of Co-trz and Co-trz-NH_2 under the specified 4-hour reaction

conditions. However, the PXRD pattern of the spent Co-trz-NH_2 showed somewhat a decrease in intensity (Figure S4), suggesting a reduction in the crystallinity of the framework after the 4-hour reaction. Additionally, SEM images revealed the spent material with pronounced roughness on the surface (Figure S5). Further prolonging irradiation time from 4 to 8 hours leads to a significant reduction in the H_2 production rate (Figure S6), which is attributed to the partial decomposition/dissolution of Co-trz-NH_2. Inductively coupled plasma optical emission spectrometry (ICP-OES) measurement indicated that 7.2% of Co^{2+} leached into the supernatant after 8 hours of irradiation. The introduction of the amino group into the framework is typically associated with a decrease in the stability of the structure, as observed in previous studies.[29, 30] This instability trend is also found in the case of Co-trz-NH_2, despite its high thermal stability, which is comparable to that of the parent Co-trz,[24] as indicated by the thermogravimetric analysis (TGA) results (Figure S7). While Co-trz-NH_2 exhibits limited stability in aqueous-based photocatalytic system, its design improves hydrogen production. This enhancement highlights the potential of this impact in the design of new photocatalyst for HER. To improve its stability in the reaction, various strategies have been proposed including modifying reaction conditions with organic solvents,[10, 23, 31] introducing hydrophobic moieties into the material to suppress the hydrolysis,[32-34] mixed-metal modification,[35, 36] core-shell method,[37] *etc*.

To verify that the reaction indeed occurs at the catalytic Co_{Td} centers within the framework rather than being restricted only on the outer surface, we prepared Co-trz-NH_2 with a smaller particle size by lowering the synthetic temperature (denoted as Co-trz-$NH_{2(small)}$, supporting information). SEM image and PXRD pattern of Co-trz-$NH_{2(small)}$ are shown in Figure S8. Co-trz-$NH_{2(small)}$ exhibits a rod-shaped morphology with lengths around 500 nm, whereas Co-trz-NH_2 displays a larger particle ranging from 1 to 2 μm in length. We performed electrochemical

measurement to determine electrical double-layer capacitance (C_{dl}), which correlates directly with outer surface area accessibility. The results, presented in Figure S9, reveal that Co-trz-$NH_{2(small)}$ has a significantly large C_{dl}, indicating a higher surface-to-volume ratio. Despite this greater outer surface area, Co-trz-$NH_{2(small)}$ exhibits lower H_2 productivity compared to Co-trz-NH_2 as summarized in Table 1 (Entry 5) and Figure S10. This finding implies that the photocatalytic reaction is taken place within the framework rather than the outer surface. Additionally, the roles of other structural attributes, *i.e.*, crystallinity, should be taken into account on the verification of their photocatalytic performances.[38-40] Crystallographic data reveal a diffraction peak at $2\theta = 10.3^{o}$, corresponding to the [100] crystal plane which is associated with the Co_{Oh} atom. The broader reflection (Figure S8b, inset) of Co-trz-$NH_{2(small)}$ indicated a lower degree of crystallinity compared to Co-trz-NH_2. This reduced crystallinity likely impedes electron transfer within the framework, leading to lower photocatalytic performance. To further investigate the impact of crystallinity, we prepared Co-trz-NH_2 with intentionally reduced crystallinity through mechanical grinding and found that the poorer crystalline phase exhibits lower H_2 production than the parent Co-trz-NH_2 compound, as shown in Figure S11. These findings underscore the impact of crystallinity on the photocatalytic activity and again confirmed that the reaction involves the entire framework not just outer surface. The observation also highlights the richness of single-atom catalytic centers (Co_{Td}) within the framework as a key factor in making Co-trz-NH_2 an effective cocatalyst for photocatalytic H_2 production.

Compared to conventional benchmarks, Co-trz-NH_2 demonstrated a hydrogen production rate that was twice as high as that of noble-metal Pt composited with conductive carbon (Pt@C) and 150 times greater than TiO_2 (Entries 6-7 and Figures S12). Notably, the photocatalytic systems of Co-trz-NH_2, Pt@C, and TiO_2 represent similar scenarios where the photoexcitation of FI occurs

at the outer surface. Subsequently, the photoexcited electrons transfer through the octahedral Co chain for Co-trz-NH_2, a graphitized carbon for Pt@C, or TiO_2 particle, to catalyze the reaction on the active sites of each material. The superior performance of noble-metal-free Co-trz-NH_2, which possesses abundant single-atom active sites, over a benchmark Pt@C and TiO_2 nanoparticles highlighted the role of the MOF as a potential HER cocatalyst.

Table 1 Photocatalytic H_2 evolution results at 4 hours under various conditions.

Entry	Cocatalyst	H_2 (mmol g^{-1}) at 4 hours	H_2 production rate (mmol g^{-1} h^{-1})
1	Co-trz	9.23 ± 0.54	3.08 ± 0.14
2	Co-trz-NH_2	27.14 ± 0.51	9.05 ± 0.13
3	-[a]	N/A	N/A
4	Co-trz-NH_2[b]	N/A	N/A
5	Co-trz-$NH_{2(small)}$[c]	20.70 ± 0.05	6.90 ± 0.01
6	Pt@C[d]	18.63 ± 0.92	4.66 ± 0.23
7	TiO_2[e]	0.24 ± N/A	0.06 ± N/A

Conditions: 10 mg cocatalyst, 17 mg FI, 3.75 mL TEA, 25 mL H_2O, irradiation with solar simulator 100 W Xe lamp (AM 1.5G), [a]no cocatalysts, [b]no FI, [c]Co-trz-NH_2 with smaller particle size obtained by microwave synthesis at 160 °C for 10 min, [d]10 mg 10% (w/w) Pt@C and [e]10 mg TiO_2 (Aeroxide® P25). The H_2 production rates were calculated based on the total mass and excluding the induction time, which lasted for an hour.

The impact of the amino substituent group was further examined through X-ray photoelectron spectroscopy (XPS) and X-ray absorption near-edge structure (XANES) measurements. Figure 2a illustrates the XPS spectra of Co 2*p* species in both Co-trz and Co-trz-

NH_2. It is observed that the binding energy of Co 2*p* (1/2 and 3/2) in Co-trz-NH_2 has shifted 0.42 eV towards lower binding energy, indicating an electron enrichment on the Co centers within the Co-trz-NH_2 framework. The Co K-edge XANES spectra of Co-trz-NH_2 and Co-trz are presented in Figure 2b, where the main edge peak corresponding to octahedral geometry and the small pre-edge peak attributed to tetrahedral Co consistently show similar characteristics for both.[24] Interestingly, a reduction in main-edge energy of Co-trz-NH_2 (by 0.2 eV) was observed compared to Co-trz. Similar to the observations in the XPS measurements, the presence of the amino group in the Co-trz-NH_2 structure enables electron delocalization to the Co centers, thereby enhancing the reduction of H^+ to form H_2 on electron-enriched Co active sites. Furthermore, it was revealed that, from a thermodynamic perspective, HER was significantly more favorable in the case of the Co-trz-NH_2 structure. The lowest unoccupied molecular orbital (LUMO) of Co-trz-NH_2 and Co-trz were determined using ultraviolet photoelectron spectroscopy (UPS) and energy gap (Figure S13-S14 and Table S1). The result in Figure 2c-d and Figure S15 indicates that the energy potential difference between the reduction of H^+ and the LUMO of Co-trz-NH_2 (0.45 eV) is greater than that of Co-trz (0.10 eV). This suggests that photoexcited electrons from the LUMO of Co-trz-NH_2 are more likely to be captured by H^+ with a greater thermodynamic driving force for HER.[41, 42]

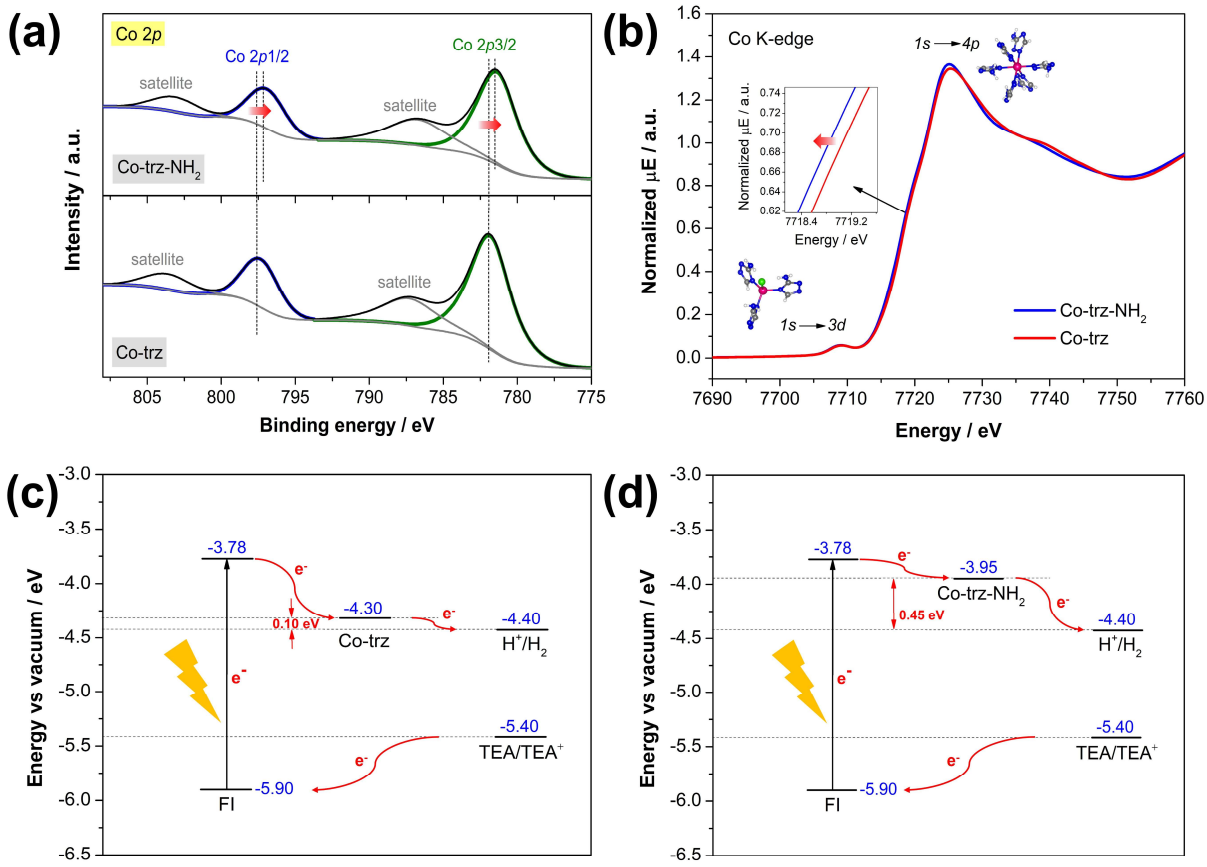

Figure 2. (a) XPS spectra of Co 2*p*, (b) Co K-Edge XANES spectra, and schematic diagram of redox potentials of (c) Co-trz,[24] and (d) Co-trz-NH_2.

In addition to modulating the electronic structure for enhanced catalytic performance, we suggest that the presence of the -NH_2 group imparts favorable characteristics to the pore channels, thereby benefiting the HER. Considering H^+ as a reactant in HER, the diffusion of H^+ within the frameworks should be one of the crucial factors influencing H_2 productivity. Pores enriched with basic -NH_2 are expected to exhibit an affinity for collecting H^+ in the solution. In other words, Co-trz-NH_2 should be able to concentrate the reactant (H^+) within the framework more effectively than pristine Co-trz. To prove this assumption, we measured the H^+ conductivity (σ) of both Co-trz-NH_2 and Co-trz using a.c. impedance spectroscopy, and the results are illustrated in Figure 3.

Co-trz-NH_2 exhibited a rapid H^+ conductivity, exceeding Co-trz by one order of magnitude across all temperatures ranging from 30-80 °C at 95% RH. The porous structure of Co-trz-NH_2, characterized by an alternative arrangement of basic amino groups, facilitates the migration of acidic H^+ within the framework, allowing it to efficiently reach the Co-active site and drive the reaction. Additionally, since the basicity of -NH_2 on the azole ligand is not particularly strong, H^+ is allowed to travel inside the pore to reach the active sites within the framework. These findings underscore the positive influence of the -NH_2 group in enhancing the photocatalytic HER performance. This enhancement is not solely attributed to the modification of the electronic structure of the parent Co-trz, but also to the role played by the NH_2 functional group as an effective pathway for the H^+ shuttle.

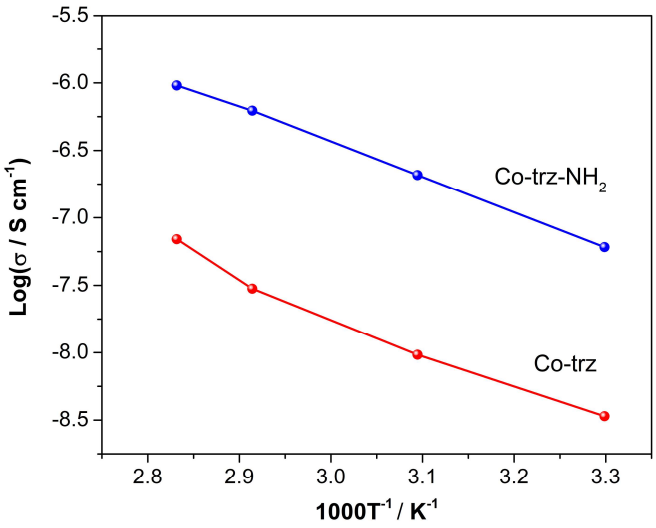

Figure 3. Variable temperature proton conductivities of Co-trz and Co-trz-NH_2 at 95 %RH.

CONCLUSION

This study elucidates the impact of the -NH_2 group on the photocatalytic hydrogen evolution performance of Co-based azolate MOF, Co-trz-NH_2. Utilizing FI photosensitizer and TEA

sacrificial agent, the Co-trz-NH_2 cocatalyst achieved a solar-driven H_2 productivity rate of 9.05 mmol g^{-1} h^{-1}. This represents a remarkable enhancement, reaching 3, 2, and 150 times higher compared to the parent Co-trz, benchmark Pt and TiO_2 cocatalysts. The amino substituent was validated for various contributions: i) tuning the electronic property leading to the enriched electron density on active Co_{Td} sites beneficial for reduction reactions, ii) facilitating H^+ diffusion within the nanopore decorated with mild basic moieties, and iii) enhancing the potential for proton reduction. These findings highlight the substantial significance of the -NH_2 group as an effective substituent for tailoring the functions of MOF-based cocatalysts, thereby serving as a potent strategy for enhancing photocatalytic H_2 evolution.

EXPERIMENTAL SECTION

Chemicals. Cobalt(II) chloride hexahydrate ($CoCl_2 \cdot 6H_2O$, 95.0%) was purchased from Ajax Finechem, Australia. 3-amino-1H-1,2,4-triazole (trz-NH_2, >99.0%), 1H-1,2,4-triazole (trz, >99.0%), fluorescein (FI, 98.0%), triethylamine (TEA, >99.0%) were purchased from Tokyo Chemical Industry, Japan, 10% (w/w) platinum loaded onto activated carbon (Pt@C), and titanium dioxide (Aeroxide® P25 TiO_2) were purchased from Sigma-Aldrich, USA. All chemicals were used as received without further purification.

Synthesis of Co-trz-NH_2. Co-trz-NH_2 was synthesized using a microwave-assisted method at 300W. A mixture of $CoCl_2 \cdot 6H_2O$ (1.29 g, 5.4 mmol) in 5 mL DI water was prepared in 35 mL microwave vials. The solution of 3-NH_2-1,2,4-trz (0.975 g, 11.6 mmol) and 5 mL of DI water were mixed and then added to the metal solution as prepared. The resulting mixture was sealed, placed in a microwave oven (CEM Discovery), and heated at 180 °C for 20 min (and 160 °C for 10 min for Co-trz-$NH_{2(small)}$ synthesis). After its synthesis, the powder was cooled to room

temperature and collected by centrifugation. Then, the sample was washed with DI water to remove unreacted organic ligands and dried under a vacuum at 40 °C overnight.

Synthesis of Co-trz. Co-trz was synthesized with a similar procedure to that described for Co-trz-NH_2 synthesis. A mixture of $CoCl_2 \cdot 6H_2O$ (0.38 g, 1.6 mmol) in 5 mL DI water was prepared in 35 mL microwave vials. The solution of 1,2,4-trz (0.23 g, 3.4 mmol) and 5 mL of DI water were mixed and then added to the metal solution. The resulting mixture was placed and heated at 160 °C for 10 min in a microwave oven (CEM Discovery). After its synthesis, the powder was cooled down to room temperature and collected by centrifugation. Then, the sample was washed with DI water and dried at 40 °C overnight.

Characterizations. The crystal phase and the crystallinity of the materials were measured using powder x-ray diffraction (PXRD) analysis on Bruker, New D8 Advance using Cu Kα radiation (λ = 1.54 Å) and counting in the range of 2θ = 5-40° at room temperature. The morphology and particle size were analyzed using a field-emission scanning electron microscope (FE-SEM, JEOL, JSM-76107). The samples were attached on carbon tape and sputtered with Pt at 10 mA under vacuum for 60 sec to increase the surface conductivity. The FTIR spectra of each sample powder were recorded using a Fourier transform infrared spectroscopy (FTIR) in the range of 400 to 2500 cm^{-1} with universal attenuated total reflectance (ATR) mode. Metal content in liquid phase was determined using inductively coupled plasma optical emission spectrometry (ICP-OES, Agilent 725) and using Argon as carrier gas. Prior to the measurement, 0.1 mL of sample was diluted to 10 mL in DI water. $CuCl_2 \cdot 2H_2O$ was used as a standard for the calibration curve (R^2 = 0.9999) at a wavelength of 230.786 nm. Thermogravimetric analysis (TGA) was performed to study the thermal behavior upon increasing temperature to 800 °C under a nitrogen atmosphere at

the flow rate of 200 cm^3 min^{-1} and ramping rate of 10 °C min^{-1} using Rigaku thermal plus evo2 (TG 8121).

X-ray Photoelectron Spectroscopy (XPS) was recorded on JEOL JPS-9010MC with a monochromatic X-ray (Al Kα source, 1486.6 eV) at 12 kV and 25 mA. All XPS spectra were measured under a high vacuum pressure of 10^{-8} Pa at room temperature. The software for running the experiment is SpecSurf ver.1.9.6. The carbon tape was coated with powder samples. The analyzed area of each sample was a cycle spot with a diameter of 6 mm. The survey scan spectra were measured with a pass energy of 50 eV, a binding energy range of 0-1100 eV and an electron-volt step of 1 eV. The narrow scan spectra were measured with a pass energy of 10 eV and an electron-volt step of 0.1 eV. The obtained spectra were evaluated using JEOL software to obtain the chemical state of the probing elements and elemental composition. All the binding energy values were referenced to the carbon peak C 1*s* at 284.70 eV. Co K-edge X-ray absorption near edge structure (XANES) measurement was performed at the BL1.1W: Multiple X-ray Techniques Beamline, Synchrotron Light Research Institute, Thailand. The measurement was conducted at ambient temperature and pressure by simultaneously measuring the samples together with the Co foil as a standard reference. The obtained data was performed using ATHENA software.[43] The optical property and energy level were performed by Ultraviolet-visible spectrometer (UV/Vis/NIR Lambda 1050 instrument, PerkinElmer) and ultraviolet photoelectron spectrometer (UPS, RIKEN KEIKI, AC-2). Protonic conductivity measurements were conducted using the electrochemical impedance spectroscopy (EIS) technique. Samples were grinded and pressed into pellets with a diameter of 5 mm and a thickness between 0.4-0.6 mm. The pellets were then sandwiched between two gold-coated electrodes. All measurements were performed in a temperature- and humidity-controlled environment using an ESPEC SH-221 temperature and

humidity chamber. The measurements were collected using a BioLogic SP-300 potentiostat over a frequency range of 1 MHz to 0.1 Hz with an input voltage amplitude of 100 mV. The collected data were analyzed using EC-Lab software V11.33 via equivalent circuit fitting. The ionic conductivity was calculated using the following equation:

$$\sigma = \frac{L}{(R) \times \pi r^2}$$

L represents the thickness of the pellet, R is the resistance, and r is the pellet radius.

Photocatalytic H_2 Evolution Experiments. A homogeneous solution of 17 mg of FI and 3.75 mL of TEA was mixed in 25 mL of DI water. Then 10 mg of Co-trz-NH_2 or Co-trz was added to the reactant mixtures and sealed with a stopper and parafilm in the closed system of a 50-mL round-bottom flash. Before the photocatalysis, the solution was degassed by N_2 gas for 1 h and in the air for 1 h. After that, the prepared samples were irradiated under a solar simulator of Xe lamp (100W, 1.5G) at 4 cm, the light distance to the solution. The H_2 products were collected at different reaction times of 0, 0.5, 1, 2, 3, and 4 h. Quantitative analysis was examined by gas chromatography (SHIMAZU, GC-2010 Plus) equipped with a SH-Rt5 Å molecular column (0.53 mm x 30 m) and barrier discharge ionization detector (BID) using He carrier gas.

In our evaluation of photocatalytic performance, we used two benchmark cocatalysts: 10 mg of 10% (w/w) platinum on activated carbon (Pt@C) and titanium dioxide (TiO_2) for comparison with our Co-trz-NH_2 catalyst.

ASSOCIATED CONTENT

The Supporting Information is available free of charge at the ACS Publications website.

Structures of Co-trz and Co-trz-NH_2, photocatalytic hydrogen evolution profiles of all MOFs as the function of time, FTIR spectroscopy, XRD patterns and SEM images of pristine and spent Co-trz-NH_2, photocatalytic performance from Co-trz-NH_2 up to 8 hours, TGA curves, SEM image and PXRD pattern of Co-trz-$NH_{2(small)}$, electrochemical active surface area (ECSA) determination, preparation of Co-trz-NH_2 with reduced crystallinity, UV-Vis and UPS spectroscopy, energy gaps and energy levels of Co-trz and Co-trz-NH_2, photocatalytic mechanisms, and recyclability test

AUTHOR INFORMATION

Corresponding Author

Sareeya Bureekaew - School of Energy Science and Engineering, Vidyasirimedhi Institute of Science and Technology, Rayong 21210, Thailand; orcid.org/0000-0001-9302-2038; E-mail: sareeya.b@vistec.ac.th

Authors

Yollada Inchongkol - School of Energy Science and Engineering, Vidyasirimedhi Institute of Science and Technology, Rayong 21210, Thailand; orcid.org/0009-0008-3229-9015

Taya Ko Saothayanun - School of Energy Science and Engineering, Vidyasirimedhi Institute of Science and Technology, Rayong 21210, Thailand; orcid.org/0000-0002-8080-9568

Kanyaporn Adpakpang - School of Energy Science and Engineering, Vidyasirimedhi Institute of Science and Technology, Rayong 21210, Thailand; orcid.org/0000-0002-1388-3389

Natchaya Phongsuk - School of Energy Science and Engineering, Vidyasirimedhi Institute of Science and Technology, Rayong 21210, Thailand; orcid.org/0009-0006-6847-2575

Sarawoot Impeng - National Nanotechnology Center (NANOTEC), National Science and Technology Development Agency (NSTDA), 111 Thailand Science Park, Pahonyothin Rd., Klong Luang, Pathum Thani 12120, Thailand; orcid.org/0000-0001-6693-1244

Soracha Kosasang - Department of Chemistry, Graduate School of Science, Kyoto University, Kitashirakawa-Oiwakecho, Sakyo-ku, Kyoto 606-8502, Japan; orcid.org/0009-0006-5254-2890

Nattapol Ma - International Center for Young Scientists (ICYS), National Institute for Materials Science, 1-1 Namiki, Tsukuba, Ibaraki, 305-0044, Japan; orcid.org/0000-0002-6162-1834

Satoshi Horike - Department of Materials Science and Engineering, School of Molecular Science and Engineering, Vidyasirimedhi Institute of Science and Technology, Rayong 21210, Thailand; orcid.org/0000-0001-8530-6364

Author Contributions

Y. I. and S. B. conceptualized and designed the experiments, Y. I., T. K. S., and S. B. cowrote the manuscript, Y. I. performed the experiments and the characterizations, and K. A. and N. P. provided assistance with the electrochemical measurements. All authors contributed to the discussions and approved the final version of the manuscript.

Notes

The authors declare no competing financial interests.

ACKNOWLEDGMENT

This work was supported by VISTEC through the program of PhD and postdoctoral fellowships, by the Program Management Unit for Human Resources & Institutional Development, Research and Innovation (Grant B05F650042), were acknowledged for the financial support (VISTEC,

FRC, *etc*.). The authors also acknowledge Prof. Dr. Makoto Ogawa for supporting instruments that have contributed to the research results and Dr. Suttipong Wannapaiboon for the technical assistance on XAS measurements.

REFERENCES

(1) Turner, J. A. Sustainable hydrogen production. *Science* **2004**, *305* (5686), 972-974.

(2) Lubitz, W.; Tumas, W. Hydrogen: an overview. *Chem. Rev.* **2007**, *107* (10), 3900-3903.

(3) Lewis, N. S.; Nocera, D. G. Powering the planet: Chemical challenges in solar energy utilization. *Proc. Natl. Acad. Sci.* **2006**, *103* (43), 15729-15735.

(4) Mao, S. S.; Chen, X. Selected nanotechnologies for renewable energy applications. *Int. J. Energy Res.* **2007**, *31* (6-7), 619-636.

(5) Lv, S.; Du, Y.; Wu, F.; Cai, Y.; Zhou, T. Review on LSPR assisted photocatalysis: effects of physical fields and opportunities in multifield decoupling. *Nanoscale Adv.* **2022**, *4* (12), 2608-2631.

(6) Tan, X.; Fang, M.; Li, J.; Lu, Y.; Wang, X. Adsorption of Eu (III) onto TiO2: effect of pH, concentration, ionic strength and soil fulvic acid. *J. Hazard. Mater.* **2009**, *168* (1), 458-465.

(7) Kumar, S. G.; Devi, L. G. Review on modified TiO2 photocatalysis under UV/visible light: selected results and related mechanisms on interfacial charge carrier transfer dynamics. *J. Phys. Chem. A.* **2011**, *115* (46), 13211-13241.

(8) Yang, J.; Wang, D.; Han, H.; Li, C. Roles of cocatalysts in photocatalysis and photoelectrocatalysis. *Acc. Chem. Res.* **2013**, *46* (8), 1900-1909.

(9) Toyao, T.; Saito, M.; Dohshi, S.; Mochizuki, K.; Iwata, M.; Higashimura, H.; Horiuchi, Y.; Matsuoka, M. Development of a Ru complex-incorporated MOF photocatalyst for hydrogen production under visible-light irradiation. *Chem. Commun.* **2014**, *50* (51), 6779-6781.

(10) Li, C.; Xu, H.; Gao, J.; Du, W.; Shangguan, L.; Zhang, X.; Lin, R.-B.; Wu, H.; Zhou, W.; Liu, X. Tunable titanium metal–organic frameworks with infinite 1D Ti–O rods for efficient visible-light-driven photocatalytic H 2 evolution. *J. Mater. Chem. A* **2019**, *7* (19), 11928-11933.

(11) Sun, D.; Liu, W.; Qiu, M.; Zhang, Y.; Li, Z. Introduction of a mediator for enhancing photocatalytic performance via post-synthetic metal exchange in metal–organic frameworks (MOFs). *Chem. Commun.* **2015**, *51* (11), 2056-2059.

(12) He, J.; Wang, J.; Chen, Y.; Zhang, J.; Duan, D.; Wang, Y.; Yan, Z. A dye-sensitized Pt@ UiO-66 (Zr) metal–organic framework for visible-light photocatalytic hydrogen production. *Chem. Commun.* **2014**, *50* (53), 7063-7066.

(13) Wang, D.; Song, Y.; Cai, J.; Wu, L.; Li, Z. Effective photo-reduction to deposit Pt nanoparticles on MIL-100 (Fe) for visible-light-induced hydrogen evolution. *New J. Chem.* **2016**, *40* (11), 9170-9175.

(14) Li, S.; Wu, F.; Lin, R.; Wang, J.; Li, C.; Li, Z.; Jiang, J.; Xiong, Y. Enabling photocatalytic hydrogen production over Fe-based MOFs by refining band structure with dye sensitization. *Chem. Eng. J.* **2022**, *429*, 132217.

(15) Wang, S.; Wang, X. Multifunctional metal–organic frameworks for photocatalysis. *small* **2015**, *11* (26), 3097-3112.

(16) Gomes Silva, C.; Luz, I.; Llabres i Xamena, F. X.; Corma, A.; García, H. Water stable Zr–benzenedicarboxylate metal–organic frameworks as photocatalysts for hydrogen generation. *Chem. Eur. J.* **2010**, *16* (36), 11133-11138.

(17) Wang, C.; DeKrafft, K. E.; Lin, W. Pt nanoparticles@ photoactive metal–organic frameworks: efficient hydrogen evolution via synergistic photoexcitation and electron injection. *J. Am. Chem. Soc.* **2012**, *134* (17), 7211-7214.

(18) Pullen, S.; Fei, H.; Orthaber, A.; Cohen, S. M.; Ott, S. Enhanced photochemical hydrogen production by a molecular diiron catalyst incorporated into a metal–organic framework. *J. Am. Chem. Soc.* **2013**, *135* (45), 16997-17003.

(19) Kataoka, Y.; Sato, K.; Miyazaki, Y.; Masuda, K.; Tanaka, H.; Naito, S.; Mori, W. Photocatalytic hydrogen production from water using porous material [Ru 2 (p-BDC) 2] n. *Energy Environ. Sci.* **2009**, *2* (4), 397-400.

(20) Guan, J.; Pal, T.; Kamiya, K.; Fukui, N.; Maeda, H.; Sato, T.; Suzuki, H.; Tomita, O.; Nishihara, H.; Abe, R. Two-dimensional metal–organic framework acts as a hydrogen evolution cocatalyst for overall photocatalytic water splitting. *ACS Catal.* **2022**, *12* (7), 3881-3889.

(21) Toyao, T.; Saito, M.; Horiuchi, Y.; Mochizuki, K.; Iwata, M.; Higashimura, H.; Matsuoka, M. Efficient hydrogen production and photocatalytic reduction of nitrobenzene over a visible-light-responsive metal–organic framework photocatalyst. *Catal. Sci. Technol.* **2013**, *3* (8), 2092-2097.

(22) Horiuchi, Y.; Toyao, T.; Saito, M.; Mochizuki, K.; Iwata, M.; Higashimura, H.; Anpo, M.; Matsuoka, M. Visible-light-promoted photocatalytic hydrogen production by using an amino-functionalized Ti (IV) metal–organic framework. *J. Phys. Chem. C.* **2012**, *116* (39), 20848-20853.

(23) Xiao, J. D.; Shang, Q.; Xiong, Y.; Zhang, Q.; Luo, Y.; Yu, S. H.; Jiang, H. L. Boosting photocatalytic hydrogen production of a metal–organic framework decorated with platinum nanoparticles: the platinum location matters. *Angew. Chem. Int. Ed.* **2016**, *55* (32), 9389-9393.

(24) Pukdeejorhor, L.; Adpakpang, K.; Wannapaiboon, S.; Bureekaew, S. Co-based metal–organic framework for photocatalytic hydrogen generation. *Chem. Commun.* **2022**, *58* (59), 8194-8197.

(25) Patel, R.; Weller, M. T.; Price, D. J. Topological ferrimagnetism and superparamagnetic-like behaviour in a disordered homometallic coordination network. *Dalton Trans.* **2007**, (36), 4034-4039.

(26) Ouellette, W.; Galán-Mascarós, J. R.; Dunbar, K. R.; Zubieta, J. Hydrothermal synthesis and structure of a three-dimensional cobalt (II) triazolate magnet. *Inorg. Chem.* **2006**, *45* (5), 1909-1911.

(27) Sözerli, Ş. E.; Özen, A.; Kani, I.; Demir, D. Synthesis and characterization of a novel 3-amino-1, 2, 4-triazole lead (II) coordination polymer. *Turk. J. Chem.* **2014**, *38* (4), 671-678.

(28) Trivedi, M. K.; Tallapragada, R. M.; Branton, A.; Trivedi, D.; Nayak, G.; Mishra, R. K.; Jana, S. Characterization of physical, spectral and thermal properties of biofield treated 1, 2, 4-Triazole. *J Mol Pharm Org Process Res* **2015**, *3* (128), 2.

(29) Chavan, S. M.; Shearer, G. C.; Svelle, S.; Olsbye, U.; Bonino, F.; Ethiraj, J.; Lillerud, K. P.; Bordiga, S. Synthesis and characterization of amine-functionalized mixed-ligand metal–organic frameworks of UiO-66 topology. *Inorg. Chem.* **2014**, *53* (18), 9509-9515.

(30) Kleist, W.; Maciejewski, M.; Baiker, A. MOF-5 based mixed-linker metal–organic frameworks: Synthesis, thermal stability and catalytic application. *Thermochim. Acta* **2010**, *499* (1-2), 71-78.

(31) Kampouri, S.; Nguyen, T. N.; Ireland, C. P.; Valizadeh, B.; Ebrahim, F. M.; Capano, G.; Ongari, D.; Mace, A.; Guijarro, N.; Sivula, K. Photocatalytic hydrogen generation from a visible-light responsive metal–organic framework system: the impact of nickel phosphide nanoparticles. *J. Mater. Chem. A* **2018**, *6* (6), 2476-2481.

(32) Ding, M.; Jiang, H.-L. Improving water stability of metal–organic frameworks by a general surface hydrophobic polymerization. *CCS Chem.* **2021**, *3* (8), 2740-2748.

(33) Ma, D.; Li, Y.; Li, Z. Tuning the moisture stability of metal–organic frameworks by incorporating hydrophobic functional groups at different positions of ligands. *Chem. Commun.* **2011**, *47* (26), 7377-7379.

(34) Yang, J.; Grzech, A.; Mulder, F. M.; Dingemans, T. J. Methyl modified MOF-5: a water stable hydrogen storage material. *Chem. Commun.* **2011**, *47* (18), 5244-5246.

(35) Yang, H.; He, X.-W.; Wang, F.; Kang, Y.; Zhang, J. Doping copper into ZIF-67 for enhancing gas uptake capacity and visible-light-driven photocatalytic degradation of organic dye. *J. Mater. Chem.* **2012**, *22* (41), 21849-21851.

(36) Zhou, K.; Mousavi, B.; Luo, Z.; Phatanasri, S.; Chaemchuen, S.; Verpoort, F. Characterization and properties of Zn/Co zeolitic imidazolate frameworks vs. ZIF-8 and ZIF-67. *J. Mater. Chem. A* **2017**, *5* (3), 952-957.

(37) Liu, X.; Li, Y.; Ban, Y.; Peng, Y.; Jin, H.; Bux, H.; Xu, L.; Caro, J.; Yang, W. Improvement of hydrothermal stability of zeolitic imidazolate frameworks. *Chem. Commun.* **2013**, *49* (80), 9140-9142.

(38) Alfonso-Herrera, L. A.; Huerta-Flores, A. M.; Martínez, L. M. T.; Ramírez-Herrera, D. J.; Rivera-Villanueva, J. M-008: A stable and reusable metalorganic framework with high crystallinity applied in the photocatalytic hydrogen evolution and the degradation of methyl orange. *J. Photochem. Photobiol. A: Chem.* **2020**, *389*, 112240.

(39) Ohtani, B.; Ogawa, Y.; Nishimoto, S.-i. Photocatalytic activity of amorphous− anatase mixture of titanium (IV) oxide particles suspended in aqueous solutions. *J. Phys. Chem. B* **1997**, *101* (19), 3746-3752.

(40) Wei, Z.; Kowalska, E.; Verrett, J.; Colbeau-Justin, C.; Remita, H.; Ohtani, B. Morphology-dependent photocatalytic activity of octahedral anatase particles prepared by ultrasonication–hydrothermal reaction of titanates. *Nanoscale* **2015**, *7* (29), 12392-12404.

(41) Guiglion, P.; Butchosa, C.; Zwijnenburg, M. A. Polymer photocatalysts for water splitting: insights from computational modeling. *Macromol. Chem. Phys.* **2016**, *217* (3), 344-353.

(42) Sprick, R. S.; Jiang, J.-X.; Bonillo, B.; Ren, S.; Ratvijitvech, T.; Guiglion, P.; Zwijnenburg, M. A.; Adams, D. J.; Cooper, A. I. Tunable organic photocatalysts for visible-light-driven hydrogen evolution. *J. Am. Chem. Soc.* **2015**, *137* (9), 3265-3270.

(43) Ravel, B.; Newville, M. ATHENA, ARTEMIS, HEPHAESTUS: data analysis for X-ray absorption spectroscopy using IFEFFIT. *J. Synchrotron Radiat.* **2005**, *12* (4), 537-541.

For Table of Contents Only